

1 **Incorporating Uncertainty into a Regression Neural**
2 **Network Enables Identification of Decadal**
3 **State-Dependent Predictability**

4 **Emily M. Gordon¹ and Elizabeth A. Barnes¹**

5 ¹Department of Atmospheric Science, Colorado State University, Fort Collins, Colorado

6 **Key Points:**

- 7 • Artificial neural networks skillfully predict sea surface temperatures on decadal
8 timescales.
- 9 • The networks identify predictability by assigning lower uncertainty to initial states
10 that lead to lower prediction error.
- 11 • More predictable initial states coincide with combinations of phases of large scale
12 decadal variability.

Corresponding author: E. M. Gordon, emily.m.gordon95@gmail.com

Abstract

Predictable internal climate variability on decadal timescales (2-10 years) is associated with large-scale oceanic processes, however these predictable signals may be masked by the noisy climate system. One approach to overcoming this problem is investigating state-dependent predictability - how differences in prediction skill depend on the initial state of the system. We present a machine learning approach to identify state-dependent predictability on decadal timescales in the Community Earth System Model version 2 by incorporating uncertainty estimates into a regression neural network. We leverage the network's prediction of uncertainty to examine state dependent predictability in sea surface temperatures by focusing on predictions with the lowest uncertainty outputs. In particular, we study two regions of the global ocean - the North Atlantic and North Pacific - and find that skillful initial states identified by the neural network correspond to particular phases of Atlantic multi-decadal variability and the interdecadal Pacific oscillation.

Plain Language Summary

As the climate warms with anthropogenic climate change, it is increasingly important to predict long term climate variability in order to prepare for possible extremes. However, the Earth's climate is chaotic and deciphering predictable long-term signals from this noisy system has proven challenging. Here we leverage times where predictable signals rise above the noise and the long-term forecasts have less error. We present a machine learning approach to identify these times when the climate is more predictable and show that these are related to particular patterns of heat in the Atlantic and Pacific Oceans.

1 Introduction

Predicting the evolution of the climate on decadal timescales (2-10 year) has far reaching implications for both climate science and society. On these timescales, changes in climate patterns are associated with either the forced response to anthropogenic emissions, or internal variability in ocean (Meehl et al., 2021). For example, the forced response from climate change can manifest as the steady increase of global mean temperature which provides some predictability of future temperatures. Decadal predictability of oceanic variability arises from the ocean's ability to store, distribute and transport heat on decadal timescales. Major modes of variability in the Pacific and Atlantic

Oceans are therefore linked to decadal predictability as they indicate the spatial distribution of heat in these basins. Furthermore, this internal variability in the ocean can act to either mask or amplify the forced response from climate change (Trenberth & Fasullo, 2013). The Pacific Ocean exhibits long-term variability via the interdecadal Pacific oscillation (IPO Power et al., 1999; Meehl et al., 2013) and its related mode Pacific decadal variability (PDV, Mantua et al., 1997; Y. Zhang et al., 1997) and the Atlantic Ocean exhibits long term variability via Atlantic multi-decadal variability (AMV, Enfield et al., 2001; Xie & Tanimoto, 1998). Because these modes of variability are associated with decadal predictability, decadal prediction is traditionally focused on either investigating and predicting the processes themselves, (e.g. Meehl et al., 2016; Gordon et al., 2021; R. Zhang et al., 2019), or exploring the predictability that arises from the atmospheric teleconnections driven by these modes (e.g. R. Zhang & Delworth, 2006; Simpson et al., 2018, 2019).

Predictability in the climate system can vary drastically depending on region, timescale, and initial state (Christensen et al., 2020; Meehl et al., 2021; Mariotti et al., 2020) thus recent studies have encouraged a shift of focus towards the concept of state-dependent predictability (Merryfield et al., 2020; Mariotti et al., 2020; Mayer & Barnes, 2021). This paradigm intrinsically acknowledges that some initial states lead to more predictable behavior than others, that is, predictability depends on the initial state of the system. The aim is therefore to identify these more predictable initial states, as they provide the opportunity to make more skillful forecasts. Examples of state-dependent predictability have been shown to exist on decadal timescales for example, it has been found that anomalously strong ocean heat transport in the North Atlantic ocean is associated with skillful predictions of sea surface temperature (SST) in the North Atlantic Subpolar Gyre for lead times up to 8 years (Brune et al., 2018; Borchert et al., 2018). So enhanced heat transport in the North Atlantic could be considered a more predictable initial state for predicting North Atlantic SSTs.

With this increased focus on state-dependent predictability, it is necessary to explore methods that can objectively identify state-dependent predictability. Machine learning is one such method that shows promise for identifying more predictable initial states. In fact, on subseasonal timescales, classification artificial neural networks (ANNs) have been shown to objectively identify states of the Madden-Julian oscillation that lead to enhanced predictability of circulation in the North Atlantic (Mayer & Barnes, 2021) by leveraging the network's confidence in a prediction to identify state-dependent predictabil-

77 ity. Furthermore, on decadal timescales it has been demonstrated that ANNs can skill-
78 fully predict decadal processes (Gordon et al., 2021; Labe & Barnes, 2022) and identify
79 states of enhanced predictability of surface temperature over land (Toms et al., 2021).

80 This study introduces the identification of state-dependent predictability on decadal
81 timescales using a regression-based neural network to predict sea surface temperatures
82 (SSTs) across the globe within the Community Earth System Model, version 2 (CESM2,
83 Danabasoglu et al., 2020). We demonstrate a powerful technique for incorporating un-
84 certainty into the prediction of regression neural networks which has previously only been
85 used a handful of times in climate science (Foster et al., 2021; Guillaumin & Zanna, 2021;
86 Barnes & Barnes, 2021). We further leverage this uncertainty output to identify which
87 initial states are associated with the lower uncertainty predictions. This allows for the
88 identification of state-dependent predictability, and furthermore, by linking predictable
89 initial states to major modes of variability, we are able to identify certain combinations
90 of IPO and AMV phases that correspond to skillful decadal forecasts.

91 **2 Data and Methods**

92 **2.1 Data**

93 We use sea surface temperature (SST) and ocean heat content (OHC) output from
94 the CESM2 pre-industrial control run for the Coupled Model Intercomparison Project
95 phase 6 (CMIP6; Eyring et al., 2016). OHC is interpolated to a $4^\circ \times 4^\circ$ grid, while SST
96 is interpolated to a $5^\circ \times 5^\circ$ grid. We use monthly output of the 2000 year run with the
97 first 100 years removed to allow the ocean circulation to spin-up. Both OHC and SST
98 are then de-seasonalized by removing the mean annual cycle from each grid point. Fur-
99 thermore, to account for model drift, after deseasonalizing we calculate the third degree
100 polynomial trend via least squares and subtract this from each grid point. This means
101 that each variable's statistics are approximately stationary for the remaining 1900 years
102 of data. OHC is smoothed using a 60 month backward running mean to smooth high
103 frequency variability. We divide the pre-processed data into training, validation and test-
104 ing. The first 70% (~ 1300 years) is used for training, the next 15% (~ 300 years) for val-
105 idation and the last 15% (~ 300 years) for testing. We calculate the mean and standard
106 deviation for every point on both the OHC and SST grids in the training set. We then
107 use these values to standardize all of the training, validation and testing data.

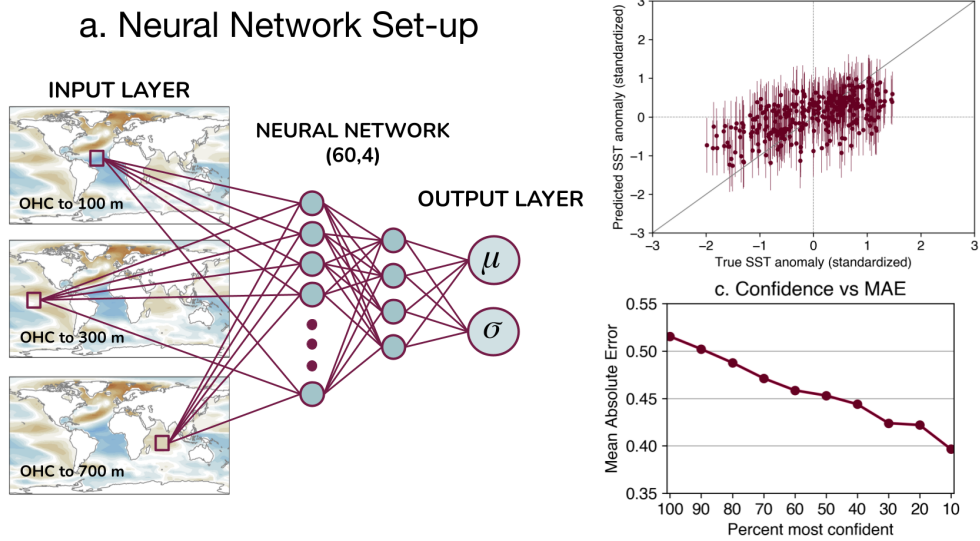


Figure 1. a. Schematic of the artificial neural network architecture. b. Scatter plot of predicted SST anomaly (y axis) vs true SST anomaly (x axis). Dots represent predicted μ values, while vertical lines represent the 1σ range. c. Prediction mean absolute error (MAE) as a function of prediction confidence (see text). Both b. and c. utilize the same network trained to predict SST in the North Atlantic Ocean (52.5°N , 325°E).

108 2.2 Artificial Neural Network

109 Artificial neural networks (ANNs) are used to predict the average SST anomaly
 110 at a lead time of 1-5 years and 3-7 years. A schematic of our neural network architec-
 111 ture is provided in Figure 1a and a brief overview of ANNs for geoscience applica-
 112 tions can be found in e.g. Toms et al. (2020). The predictors are three OHC grids, where each
 113 grid is OHC integrated to a different depth (100 m, 300 m and 700 m). We chose vary-
 114 ing depths of OHC because each contains information corresponding to different forms
 115 of climate variability. For example, the upper levels of the ocean integrate atmospheric
 116 forcing, and hence capture atmospheric variability as well as surface ocean dynamics (Frankignoul
 117 & Hasselmann, 1977). The variability in lower levels of the ocean is guided by a com-
 118 bination of slow moving ocean circulation and the incorporation of mixed layer processes
 119 via the annual cycle in the thermocline (Alexander & Deser, 1995). By inputting three
 120 OHC depths into the neural network, it can theoretically combine different oceanic and
 121 atmospheric processes to make its predictions. The three ocean grids are vectorized with
 122 points over land removed resulting in a total 7947 input pixels. This input is densely con-
 123 nected to a hidden layer of 60 nodes which is then densely connected to another hidden
 124 layer of 4 nodes (see Fig.1). All nodes in the hidden layers use the rectified linear unit
 125 (ReLU) activation function. Finally this second layer is connected to the output layer
 126 of two nodes which serve as the parameters of the predicted conditional distribution (see
 127 details in the next paragraph). Here the distribution is a normal distribution as we found
 128 allowing skewness did not significantly improve the network’s performance (not shown).

129 We use the $-\log(p)$ loss function described by e.g. Barnes et al. (2021) which we
 130 will summarize briefly. For each input, the network outputs two values, μ and σ . To cal-
 131 culate loss, μ and σ are used to construct a conditional distribution, d and the negative
 132 log likelihood function is calculated at the true value (y_{true}), i.e. $\text{loss} = -\log(p(y_{true}|d))$.
 133 This means that the neural network can decrease loss (decrease $-\log(p(y_{true}|d))$) in dif-
 134 ferent ways: either with a low σ value and μ that is close to y_{true} , or predict a larger
 135 σ value with μ that is further from y_{true} , or both. The neural network is therefore not
 136 penalized for high error predictions as long as it also guesses a correspondingly high σ
 137 value, that is, if it recognizes an input is less predictable by assigning a high σ value. The
 138 predictions of such an ANN are illustrated in Figure 1b, where we show an example scat-
 139 ter plot of prediction vs truth from an ANN trained to predict SST anomaly in the North
 140 Atlantic Subpolar Gyre. Note that we can plot both the predicted anomaly value (μ , col-

141 ored dots) and an uncertainty range, with the error bars indicating the $\pm 1\sigma$ range pre-
142 dicted by the ANN. During training, we use a learning rate of 1×10^{-4} with stochastic
143 gradient descent for up to 1000 epochs with early stopping when validation loss did not
144 decrease for 100 epochs. To implement regularization, we include a dropout layer between
145 the input layer and first hidden layer in training. We found that a high rate of dropout
146 (80% dropout rate in this experiment) forced the ANN to learn information more slowly
147 and greatly reduced over-fitting on the validation set.

148 **2.3 AMV and IPO indices**

149 We compute the AMV and IPO indices within CESM2 using the deseasoned and
150 detrended SST data. For the AMV index, we calculate the monthly mean SST anomaly
151 over the North Atlantic ocean (0°N to 80°N , 280°E to 360°E) and then standardize by
152 removing the mean and dividing by the standard deviation. Note we do not de-trend by
153 the global mean SST as recommended by Trenberth and Shea (2006) because the con-
154 trol run lacks a forced long term warming trend and model drift was removed during pre-
155 processing. We calculate the IPO index following the tripole index proposed by Henley
156 et al. (2015). We include plots of the spatial AMV and IPO patterns calculated by these
157 methods in CESM2 in Supplemental Figure 1.

158 **3 Results**

159 **3.1 Evaluating Performance**

160 In this study, 10 networks (identical architecture, only varying the initial network
161 random seed) are trained at each SST grid point in the ocean and we show the results
162 of the best neural network at each grid point. To designate the “best” network, we se-
163 lect the ANN with the lowest mean absolute error (MAE, difference between predicted
164 μ and true y) on the 10% of samples with the lowest σ predictions in the validation set.
165 This means that the network has learned to identify more predictable inputs by assign-
166 ing them low σ values, and achieves low error on these same predictions. With this des-
167 ignation, we are leveraging a fundamental characteristic of the ANN predictions: pre-
168 diction error should decrease as predicted σ decreases, so we refer to lower σ predictions
169 as more confident predictions. This is demonstrated in Figure 1c where we show a net-
170 work trained to predict SST in 1-5 years in the North Atlantic (52.5°N , 325°E). Along

171 the x-axis, we threshold by increasing confidence with the y-axis showing correspond-
 172 ing MAE for those predictions. For all samples, the MAE is ~ 0.52 however for the 40%
 173 most confident predictions the MAE has dropped to 0.46. For the 10% most confident
 174 predictions, the MAE has dropped further to ~ 0.39 . This is evidence that the ANN has
 175 learned particular input samples, or climate states, whose evolution leads to lower un-
 176 certainty. Although we choose the best network to present here, the results are largely
 177 unchanged if we instead select the mean across all 10 networks. For some initial random
 178 seeds, the network fails to learn anything and always predicts zero (or very close to zero).
 179 These networks are removed before analysis.

180 3.2 Predicting SST

181 We ensure that the ANNs are learning to skillfully predict SSTs on decadal timescales
 182 by examining prediction error in the testing data at each grid point. Fig. 2a is the MAE
 183 for ANN predictions for the testing set for lead years 1-5, with black indicating grid points
 184 where all 10 networks failed to learn anything. The lowest MAEs are found in the North
 185 Atlantic Ocean, North Pacific Ocean, and the Southern Ocean around South America.
 186 This spatial distribution of prediction skill broadly agrees with that found in the decadal
 187 hindcast studies using the CESM1 decadal prediction large ensemble (Yeager et al., 2018;
 188 Christensen et al., 2020), which suggests that the spatially varying predictability is not
 189 a result of experiment design or network architecture. The prediction skill for lead years
 190 3-7 is shown in Fig. 2b and highlights similar regions as being more predictable as in lead
 191 years 1-5. Furthermore, there does not seem to be a substantial loss in skill between these
 192 two lead times. This, coupled with the spatial spread of predictability, suggests that the
 193 ANNs are learning physical relationships to make their predictions.

194 To contextualize the predictions of the ANNs, we benchmark them against a sim-
 195 ple persistence model. The persistence model predicts that the SST anomaly will be un-
 196 changed so that the SST anomaly at the time of input remains the same at the time of
 197 prediction. We calculate the MAE for the persistence model and subtract it from the
 198 MAE of the ANNs ($\Delta\text{MAE} = \text{MAE}_{ANN} - \text{MAE}_{persistence}$), and plot the results in Fig-
 199 ure 2e and 2f. In regions where ΔMAE is more negative, the ANN outperforms persis-
 200 tence (i.e. has lower error). These regions are illustrated in warm colors in Figure 2e and
 201 2f and illustrates that the ANNs trained in this study out-perform persistence in all lo-
 202 cations and at both lead times. The greatest improvement in skill above persistence oc-

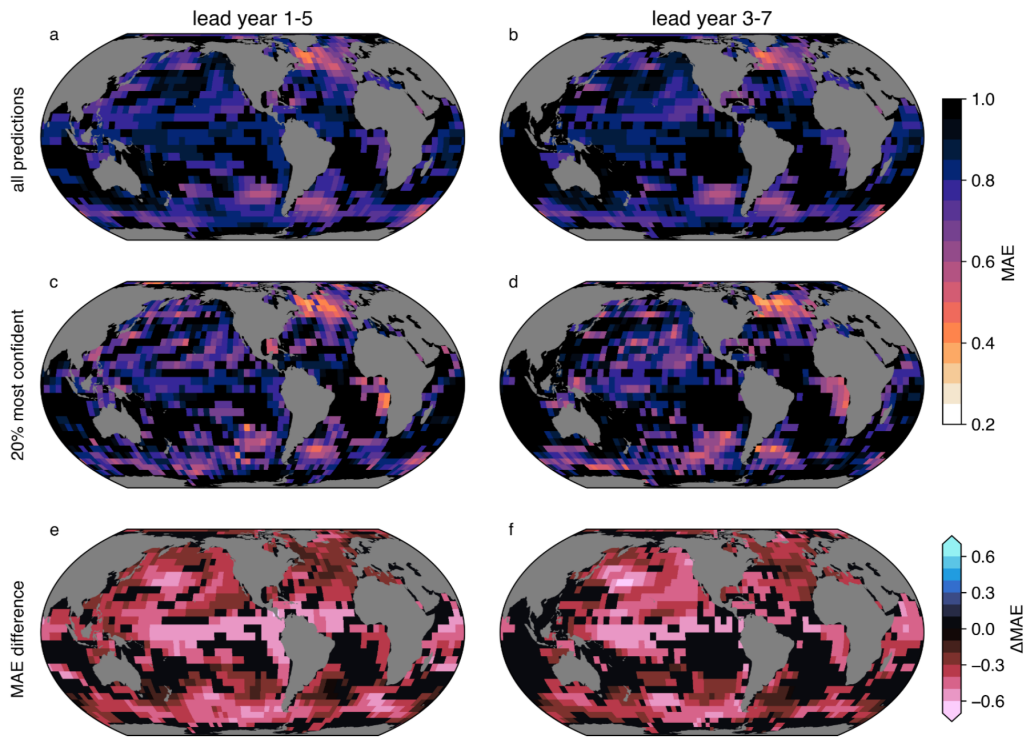


Figure 2. Evaluation of ANN prediction error. Left column is for lead year 1-5, and right column for lead year 3-7. Panel a and panel b are mean absolute error (MAE) for all predictions in the testing set. Panel c and panel d show MAE for only the 20% most confident predictions in the testing set as identified using the ANNs’s uncertainty. Panel e and panel f are the difference between MAE_{ANN} and $MAE_{persistence}$ ($MAE_{ANN} - MAE_{persistence}$) in the testing set.

203 curs in the cold tongue region of the Equatorial Pacific. This is unsurprising as this re-
204 gion exhibits large interannual variability due to the El Nino Southern Oscillation, and
205 hence persistence performs poorly in this region.

206 **3.3 Identifying State-Dependent Predictability**

207 The predictive power of ANNs for decadal prediction is now demonstrated by us-
208 ing them to identify state-dependent predictability. In Figure 2c and 2d we plot the MAE
209 for only the 20% most confident predictions (20% lowest predicted σ) by the ANN for
210 each SST grid point. That is, ANN objectively identifies more predictable initial states,
211 and we do not directly use knowledge of the ground truth to identify these predictions.
212 When comparing the most confident predictions with all predictions (Fig 2c with 2a),
213 MAE is reduced everywhere for more confident predictions, implying that more confi-
214 dent predictions are associated with smaller prediction errors at all locations. Similarly
215 for lead year 3-7 (Figs. 2b and 2d) we see that sorting for the most confident predictions
216 leads to reduced error at all locations. Interestingly, at both lead times, some regions that
217 show very little skill across all predictions exhibit large increases in skill when consid-
218 ering only the most confident predictions (e.g. central Pacific and the Gulf of Guinea),
219 demonstrating that a region may be considered not predictable when in fact it is just
220 not *always* predictable.

221 **3.4 Investigating Skillful Decadal Predictions**

222 By using ANN predictions to identify state dependent predictability, we can also
223 investigate oceanic patterns that lead to predictability. Here we examine the predictions
224 of two ANNs trained to predict SSTs in the North Atlantic and North Pacific oceans to
225 investigate processes that are contributing to enhanced prediction skill in these regions.
226 Figure 3 shows the 20% most confident predictions of positive SST anomaly for a point
227 in the North Atlantic Sub-Polar Gyre (52.5°N, 325°E). We single out positive predic-
228 tions because the ANN's confident predictions are preferentially positive (583 positive
229 predictions out of 680 confident testing samples), implying that the ANN detects that
230 particular positive predictions lead to lower uncertainty. Here, we plot the correct and
231 confident positive predictions to ensure we are analyzing the correct signals that con-
232 tribute to predictability. This leaves 472 samples. Fig 3a – 3c show the composite of OHC
233 input maps for correct and confident positive predictions to investigate the initial states

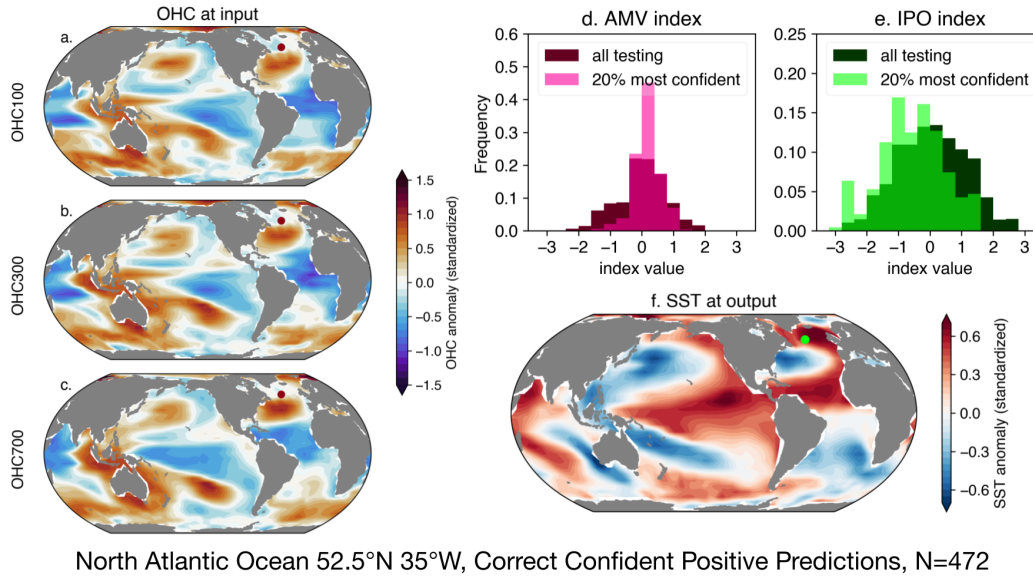


Figure 3. State-dependent predictability identified in the North Atlantic. Panels a-c: Composite of OHC inputs for confident predictions of positive SST anomaly in a point in the North Atlantic (red dot). Panel d: histogram of AMV index for testing data (dark pink) and most confident predictions (light pink). Panel e: as panel d but for IPO index. Panel f: Composite of SST map for confident predictions of SST in the North Atlantic (red dot).

234 that lead to predictability. At all three OHC levels there is a positive OHC anomaly in
 235 the subtropical to mid-latitude Atlantic Ocean. We verify that this signal was likely uti-
 236 lized by the ANN in its predictions by using an ANN explainability technique to inves-
 237 tigate the input regions that are important to the network’s prediction (see Text S1 and
 238 Figure S2). This shows the positive OHC anomaly in the North Atlantic at all three OHC
 239 levels was highlighted as contributing to the ANN’s decisions. As the positive heat anomaly
 240 is slightly south of the predicted grid point, this could indicate northward heat trans-
 241 port to achieve a positive prediction. The composite SST anomaly in Fig 3 shows the
 242 positive anomaly is around the predicted grid point in the North Atlantic which implies
 243 that this anomaly has moved northward from the initial state. From this evidence, we
 244 posit that the skillful SST prediction is preceded by a positive heat anomaly in North
 245 Atlantic ocean, which is transported into the gyre region. This is consistent with Borchert
 246 et al. (2018) who identified periods of enhanced heat transport in the mid-latitude as a
 247 state of increased predictability of SSTs in the North Atlantic subpolar gyre for up to
 248 8 years.

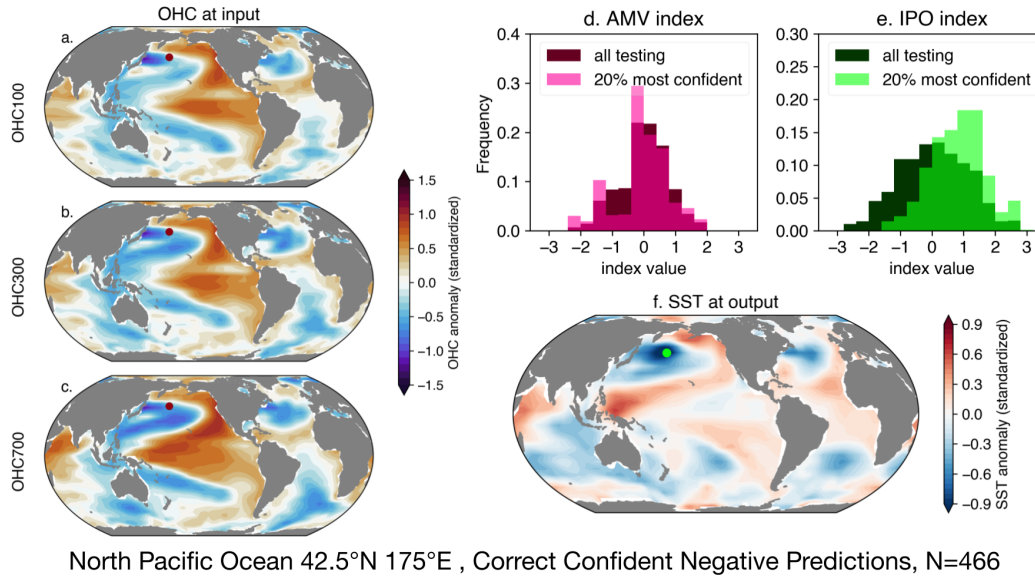


Figure 4. As Figure 3 but for the North Pacific

249 As an analogue for oceanic variability, we also consider the phases of the AMV and
 250 IPO during periods of increased network confidence. In Fig 3d we present the distribu-
 251 tion of the AMV index during the entire testing period (dark pink, mean = 0.00) with
 252 the light pink showing the distribution for only 20% confident predictions which has a
 253 mean of 0.16. From this, it appears that confident predictions are most likely to occur
 254 during positive AMV. When randomly drawing 20% of the samples from the AMV dis-
 255 tribution in testing, the likelihood of a mean of 0.16 occurring is less than 1%. This im-
 256 plies that more skillful SST predictions in the North Atlantic Sub-Polar Gyre coincide
 257 with northward heat transport from the subtropics (from 3a-c and f) coupled with the
 258 positive phase of AMV (from 3d). This is consistent with previous results by e.g. Christensen
 259 et al. (2020); Borchert et al. (2018). In 3e, we show the distribution of IPO phase for the
 260 testing data (dark green, mean = 0.05) and 20% most confident predictions in light green,
 261 with a mean of -0.58. The likelihood drawing a mean of -0.58 from the IPO testing dis-
 262 tribution is less than 1% which suggests that the negative phase of the IPO contributes
 263 to the predictability of North Atlantic SSTs. This is also apparent in Fig 3a-c which all
 264 show the negative IPO pattern in the Pacific Ocean. This may indicate some inter-basin
 265 teleconnection that contributes to the predictability of North Atlantic SSTs.

266 We now perform a similar analysis for an ANN trained to predict SST in 1-5 years
 267 at a point in the North Pacific (42.5°N, 175°E). In Figure 4 we show the results for the

268 20% most confident negative predictions. For this region, 632 out of the 680 most con-
269 fident samples were predictions of negative anomaly, implying the ANN designated neg-
270 ative predictions as more confident. Again we plot only the correct predictions, result-
271 ing in 466 samples in these composites. Fig 4a-c shows the composite OHC inputs for
272 confident negative predictions, and the major signal appears to be a positive IPO/PDV
273 pattern in all panels. It is likely the ANN utilized this pattern to make these confident
274 negative predictions from the ANN explainability heat-maps (see Text S1 and Figure S3).
275 This is supported by the histogram of the IPO index in Fig 4e which shows the distri-
276 bution of IPO phase in the confident samples is shifted such that confident samples sig-
277 nificantly coincide with the positive phase of the IPO. There is no such strong signal in
278 the AMV index (Fig 4d). Lastly, it appears that the confident predictions appear to re-
279 late to persistence in the positive IPO phase because the composite map of SST at out-
280 put (Fig 4f) shows an IPO pattern in the Pacific Ocean. From this, we posit that skill-
281 ful predictions of SST in the North Pacific are associated with persistence in the pos-
282 itive phase of IPO (i.e. negative SST anomaly at the predicted grid point). Here, the
283 ANN preferentially identifies negative SST predictions as skillful, perhaps implying that
284 persistence in the positive phase of IPO is more predictable than persistence of the neg-
285 ative phase.

286 4 Discussion & Conclusion

287 We show that artificial neural networks (ANNs) skillfully predict SST evolution on
288 decadal timescales and that they can objectively identify decadal state-dependent pre-
289 dictability. Specifically, we use a regression neural network where the predictions take
290 the form of a conditional normal distribution which we leverage to isolate predictions
291 that are more likely to have lower error. This approach allows us to investigate possi-
292 ble contributing mechanisms to decadal SST predictability, particularly Atlantic multi-
293 decadal variability and the interdecadal Pacific oscillation (AMV and IPO, Figs 3 and
294 4). We chose to model the conditional distributions as normal distributions as alterna-
295 tives did not significantly improve skill. We suggest that future studies investigating state-
296 dependent predictability for other timescales and variables may benefit from the addi-
297 tion of skewness to the predicted conditional distributions (Barnes et al., 2021), as well
298 as further exploring alternative network architectures to tease out additional skill.

299 We investigate state-dependent predictability in two regions, the North Atlantic
300 Subpolar Gyre, and the North Pacific Ocean by identifying predictions in these regions
301 that the ANNs assigned the lowest uncertainty and investigating the processes that cor-
302 respond to these confident predictions. This study utilizes the CESM2 long control rep-
303 resentation of the climate system and the results in the North Atlantic appear to agree
304 with hindcast studies of Brune et al. (2018); Borchert et al. (2018); Yeager et al. (2018)
305 which use different models to that used here (MPI-ESM; Giorgetta et al. (2013) and CESM1;
306 Hurrell et al. (2013)). These previous studies also incorporate observations or reanaly-
307 sis to evaluate the prediction skill of the decadal hindcasts. Since our findings are con-
308 sistent with the state-dependent predictability investigated in these studies, this suggests
309 that the ANN predictions and mechanisms investigated here are likely relevant to real-
310 istic climate variability. This is left for future work.

311 Here we present a data-driven approach to diagnosing state-dependent predictabil-
312 ity in an unforced model simulation. We find evidence for a state-dependent inter-basin
313 teleconnection, that is, the negative phase of the IPO influencing predictability of North
314 Atlantic SSTs (Fig 3). The drivers of predictability and variability in the North Atlantic
315 ocean are still debated, especially the relative roles of internal variability and external
316 forcing (Wu et al., 2011; Clement et al., 2015; R. Zhang et al., 2019; Mann et al., 2021;
317 Fang et al., 2021; Fenske & Clement, 2022). We hence suggest that future work on decadal
318 prediction should investigate the roles of internal variability and external forcing through
319 the lens of state-dependent predictability.

320 This study emphasizes the importance of examining state-dependent predictabil-
321 ity for decadal predictions. We stress that the *a priori* identification of more predictable
322 initial states greatly increases prediction skill and can hence aid in estimating the evo-
323 lution of the internal long-term variability of the climate system.

324 5 Open Research

325 We use CESM2 output which is freely available from Earth System Grid [https://esgf-](https://esgf-node.llnl.gov/projects/cmip6)
326 [node.llnl.gov/projects/cmip6](https://esgf-node.llnl.gov/projects/cmip6) (Danabasoglu, 2019).

327 Analysis was carried out in Python 3.7 and 3.9, ANNs were developed using Ten-
328 sorFlow (Abadi et al., 2016), while XAI heatmaps were created with iNNvestigate (Alber
329 et al., 2019). Many color maps in this work are the from CMasher package (van der Velden,

330 2020) and regridding was achieved using Climate Data Operators (CDO; Schulzweida,
331 2019).

332 Code used to preprocess, generate the ANNs, and produce the figures in this work
333 can be found at Gordon (2022).

334 **Acknowledgments**

335 E. M. Gordon is partially funded by Fulbright New Zealand. E. M. Gordon and E. A.
336 Barnes are supported, in part, by NSF CAREER AGS-1749261 under the Climate and
337 Large-scale Dynamics program. We thank John Fasullo at the National Center for At-
338 mospheric Research (NCAR) for diagnosing the OHC from CESM2. We would like to
339 acknowledge high-performance computing support from Cheyenne (<https://doi.org/10.5065/D6RX99HX>)
340 provided by NCAR's Computational and Information Systems Laboratory, sponsored
341 by the National Science Foundation

342 **References**

- 343 Abadi, M., Barham, P., Chen, J., Chen, Z., Davis, A., Dean, J., ... Zheng, X.
344 (2016, November). Tensorflow: A system for large-scale machine learning.
345 In *12th USENIX symposium on operating systems design and implementation*
346 (*OSDI 16*) (pp. 265–283). Savannah, GA: USENIX Association. Retrieved
347 from [https://www.usenix.org/conference/osdi16/technical-sessions/](https://www.usenix.org/conference/osdi16/technical-sessions/presentation/abadi)
348 [presentation/abadi](https://www.usenix.org/conference/osdi16/technical-sessions/presentation/abadi)
- 349 Alber, M., Lapuschkin, S., Seegerer, P., Hägele, M., Schütt, K. T., Montavon, G., ...
350 Kindermans, P.-J. (2019). Investigate neural networks! *Journal of Machine*
351 *Learning Research*, *20*(93), 1-8. Retrieved from [http://jmlr.org/papers/](http://jmlr.org/papers/v20/18-540.html)
352 [v20/18-540.html](http://jmlr.org/papers/v20/18-540.html)
- 353 Alexander, M. A., & Deser, C. (1995, January). A Mechanism for the Recurrence
354 of Wintertime Midlatitude SST Anomalies. *J. Phys. Oceanogr.*, *25*(1), 122–
355 137. Retrieved from [https://journals.ametsoc.org/view/journals/phoc/](https://journals.ametsoc.org/view/journals/phoc/25/1/1520-0485_1995_025_0122_amftro_2_0_co_2.xml?tab_body=fulltext)
356 [25/1/1520-0485_1995_025_0122_amftro_2_0_co_2.xml?tab_body=fulltext](https://journals.ametsoc.org/view/journals/phoc/25/1/1520-0485_1995_025_0122_amftro_2_0_co_2.xml?tab_body=fulltext)
357 [-display](https://journals.ametsoc.org/view/journals/phoc/25/1/1520-0485_1995_025_0122_amftro_2_0_co_2.xml?tab_body=fulltext) doi: 10.1175/1520-0485(1995)025<0122:AMFTRO>2.0.CO;2
- 358 Barnes, E. A., & Barnes, R. J. (2021, December). Controlled abstention neural
359 networks for identifying skillful predictions for regression problems. *J. Adv.*
360 *Model. Earth Syst.*, *13*(12). Retrieved from <https://onlinelibrary.wiley>

- 361 .com/doi/10.1029/2021MS002575 doi: 10.1029/2021ms002575
- 362 Barnes, E. A., Barnes, R. J., & Gordillo, N. (2021, September). *Adding Uncer-*
 363 *tainty to Neural Network Regression Tasks in the Geosciences*. Retrieved from
 364 <http://arxiv.org/abs/2109.07250>
- 365 Borchert, L. F., Müller, W. A., & Baehr, J. (2018, September). Atlantic Ocean
 366 Heat Transport Influences Interannual-to-Decadal Surface Temperature Pre-
 367 dictability in the North Atlantic Region. *J. Clim.*, *31*(17), 6763–6782. Re-
 368 trieved from [https://journals.ametsoc.org/view/journals/clim/31/17/](https://journals.ametsoc.org/view/journals/clim/31/17/jcli-d-17-0734.1.xml)
 369 [jcli-d-17-0734.1.xml](https://journals.ametsoc.org/view/journals/clim/31/17/jcli-d-17-0734.1.xml) doi: 10.1175/JCLI-D-17-0734.1
- 370 Brune, S., Düsterhus, A., Pohlmann, H., Müller, W. A., & Baehr, J. (2018, Septem-
 371 ber). Time dependency of the prediction skill for the North Atlantic sub-
 372 polar gyre in initialized decadal hindcasts. *Clim. Dyn.*, *51*(5), 1947–1970.
 373 Retrieved from <https://doi.org/10.1007/s00382-017-3991-4> doi:
 374 10.1007/s00382-017-3991-4
- 375 Christensen, H. M., Berner, J., & Yeager, S. (2020, September). The Value of
 376 Initialization on Decadal Timescales: State-Dependent Predictability in the
 377 CESM Decadal Prediction Large Ensemble. *J. Clim.*, *33*(17), 7353–7370. Re-
 378 trieved from [https://journals.ametsoc.org/jcli/article/33/17/7353/](https://journals.ametsoc.org/jcli/article/33/17/7353/348619/The-Value-of-Initialization-on-Decadal-Timescales)
 379 [348619/The-Value-of-Initialization-on-Decadal-Timescales](https://journals.ametsoc.org/jcli/article/33/17/7353/348619/The-Value-of-Initialization-on-Decadal-Timescales) doi:
 380 10.1175/JCLI-D-19-0571.1
- 381 Clement, A., Bellomo, K., Murphy, L. N., Cane, M. A., Mauritsen, T., Rädel, G.,
 382 & Stevens, B. (2015, October). The Atlantic Multidecadal Oscillation with-
 383 out a role for ocean circulation. *Science*, *350*(6258), 320–324. Retrieved
 384 from <https://science.sciencemag.org/content/350/6258/320> doi:
 385 10.1126/science.aab3980
- 386 Danabasoglu, G. (2019). *Ncar cesm2 model output prepared for cmip6 cmip his-*
 387 *torical*. Earth System Grid Federation. Retrieved from [https://doi.org/10](https://doi.org/10.22033/ESGF/CMIP6.7627)
 388 [.22033/ESGF/CMIP6.7627](https://doi.org/10.22033/ESGF/CMIP6.7627) doi: 10.22033/ESGF/CMIP6.7627
- 389 Danabasoglu, G., Lamarque, J.-F., Bacmeister, J., Bailey, D. A., DuVivier, A. K.,
 390 Edwards, J., . . . Strand, W. G. (2020). The Community Earth System Model
 391 Version 2 (CESM2). *Journal of Advances in Modeling Earth Systems*, *12*(2),
 392 e2019MS001916. Retrieved from [https://agupubs.onlinelibrary.wiley](https://agupubs.onlinelibrary.wiley.com/doi/abs/10.1029/2019MS001916)
 393 [.com/doi/abs/10.1029/2019MS001916](https://agupubs.onlinelibrary.wiley.com/doi/abs/10.1029/2019MS001916) doi: 10.1029/2019MS001916

- 394 Enfield, D. B., Mestas-Nuñez, A. M., & Trimble, P. J. (2001). The Atlantic Mul-
395 tidecadal Oscillation and its relation to rainfall and river flows in the conti-
396 nental U.S. *Geophys. Res. Lett.*, *28*(10), 2077–2080. Retrieved from [http://](http://agupubs.onlinelibrary.wiley.com/doi/abs/10.1029/2000GL012745)
397 agupubs.onlinelibrary.wiley.com/doi/abs/10.1029/2000GL012745 doi:
398 10.1029/2000GL012745
- 399 Eyering, V., Bony, S., Meehl, G. A., Senior, C. A., Stevens, B., Stouffer, R. J., &
400 Taylor, K. E. (2016). Overview of the Coupled Model Intercomparison Project
401 Phase 6 (CMIP6) experimental design and organization. *Geoscientific Model*
402 *Development*, *9*(5), 1937–1958. Retrieved from [https://gmd.copernicus](https://gmd.copernicus.org/articles/9/1937/2016/)
403 [.org/articles/9/1937/2016/](https://gmd.copernicus.org/articles/9/1937/2016/) doi: 10.5194/gmd-9-1937-2016
- 404 Fang, S.-W., Khodri, M., Timmreck, C., Zanchettin, D., & Jungclaus, J. (2021,
405 December). Disentangling internal and external contributions to Atlantic
406 multidecadal variability over the past millennium. *Geophys. Res. Lett.*,
407 *48*(23). Retrieved from [https://onlinelibrary.wiley.com/doi/10.1029/](https://onlinelibrary.wiley.com/doi/10.1029/2021GL095990)
408 [2021GL095990](https://onlinelibrary.wiley.com/doi/10.1029/2021GL095990) doi: 10.1029/2021gl095990
- 409 Fenske, T., & Clement, A. (2022, February). No internal connections detected be-
410 tween low frequency climate modes in north Atlantic and north Pacific basins.
411 *Geophys. Res. Lett.*. Retrieved from [https://onlinelibrary.wiley.com/](https://onlinelibrary.wiley.com/doi/10.1029/2022GL097957)
412 [doi/10.1029/2022GL097957](https://onlinelibrary.wiley.com/doi/10.1029/2022GL097957) doi: 10.1029/2022gl097957
- 413 Foster, D., Gagne, D. J., II, & Whitt, D. B. (2021, December). Probabilistic ma-
414 chine learning estimation of ocean mixed layer depth from dense satellite and
415 sparse in situ observations. *J. Adv. Model. Earth Syst.*, *13*(12). Retrieved
416 from <https://onlinelibrary.wiley.com/doi/10.1029/2021MS002474> doi:
417 10.1029/2021ms002474
- 418 Frankignoul, C., & Hasselmann, K. (1977). Stochastic climate models, Part II
419 Application to sea-surface temperature anomalies and thermocline vari-
420 ability. *Tell'Us*, *29*(4), 289–305. Retrieved from [http://onlinelibrary](http://onlinelibrary.wiley.com/doi/abs/10.1111/j.2153-3490.1977.tb00740.x)
421 [.wiley.com/doi/abs/10.1111/j.2153-3490.1977.tb00740.x](http://onlinelibrary.wiley.com/doi/abs/10.1111/j.2153-3490.1977.tb00740.x) doi:
422 10.1111/j.2153-3490.1977.tb00740.x
- 423 Giorgetta, M. A., Jungclaus, J., Reick, C. H., Legutke, S., Bader, J., Böttinger,
424 M., ... Stevens, B. (2013, July). Climate and carbon cycle changes from
425 1850 to 2100 in MPI-ESM simulations for the Coupled Model Intercomparison
426 Project phase 5. *J. Adv. Model. Earth Syst.*, *5*(3), 572–597. Retrieved from

- 427 <http://doi.wiley.com/10.1002/jame.20038> doi: 10.1002/jame.20038
- 428 Gordon, E. M. (2022, March). *emily-gordy/Decadal-SST-prediction: Decadal SST*
 429 *prediction GRL submission*. Zenodo. Retrieved from [https://doi.org/10](https://doi.org/10.5281/zenodo.6344810)
 430 [.5281/zenodo.6344810](https://doi.org/10.5281/zenodo.6344810) doi: 10.5281/zenodo.6344810
- 431 Gordon, E. M., Barnes, E. A., & Hurrell, J. W. (2021, November). Oceanic
 432 harbingers of Pacific decadal oscillation predictability in CESM2 de-
 433 tected by neural networks. *Geophys. Res. Lett.*, *48*(21). Retrieved from
 434 <https://onlinelibrary.wiley.com/doi/10.1029/2021GL095392> doi:
 435 [10.1029/2021gl095392](https://doi.org/10.1029/2021gl095392)
- 436 Guillaumin, A. P., & Zanna, L. (2021, September). Stochastic-deep learning pa-
 437 rameterization of ocean momentum forcing. *J. Adv. Model. Earth Syst.*,
 438 *13*(9). Retrieved from [https://onlinelibrary.wiley.com/doi/10.1029/](https://onlinelibrary.wiley.com/doi/10.1029/2021MS002534)
 439 [2021MS002534](https://doi.org/10.1029/2021ms002534) doi: 10.1029/2021ms002534
- 440 Henley, B. J., Gergis, J., Karoly, D. J., Power, S., Kennedy, J., & Folland, C. K.
 441 (2015, December). A Tripole Index for the Interdecadal Pacific Oscillation.
 442 *Clim. Dyn.*, *45*(11), 3077–3090. Retrieved from [https://doi.org/10.1007/](https://doi.org/10.1007/s00382-015-2525-1)
 443 [s00382-015-2525-1](https://doi.org/10.1007/s00382-015-2525-1) doi: 10.1007/s00382-015-2525-1
- 444 Hurrell, J. W., Holland, M. M., Gent, P. R., Ghan, S., Kay, J. E., Kushner, P. J.,
 445 ... Marshall, S. (2013, September). The Community Earth System Model:
 446 A Framework for Collaborative Research. *Bull. Am. Meteorol. Soc.*, *94*(9),
 447 1339–1360. Retrieved from [https://journals.ametsoc.org/view/journals/](https://journals.ametsoc.org/view/journals/bams/94/9/bams-d-12-00121.1.xml)
 448 [bams/94/9/bams-d-12-00121.1.xml](https://doi.org/10.1175/BAMS-D-12-00121.1) doi: 10.1175/BAMS-D-12-00121.1
- 449 Labe, Z. M., & Barnes, E. A. (2022, February). *Predicting slowdowns in*
 450 *decadal climate warming trends with explainable neural networks*. Retrieved
 451 from <http://www.essoar.org/doi/10.1002/essoar.10508874.2> doi:
 452 [10.1002/essoar.10508874.2](https://doi.org/10.1002/essoar.10508874.2)
- 453 Mann, M. E., Steinman, B. A., Brouillette, D. J., & Miller, S. K. (2021, March).
 454 Multidecadal climate oscillations during the past millennium driven by vol-
 455 canic forcing. *Science*, *371*(6533), 1014–1019. Retrieved from [http://](http://dx.doi.org/10.1126/science.abc5810)
 456 [dx.doi.org/10.1126/science.abc5810](https://doi.org/10.1126/science.abc5810) doi: 10.1126/science.abc5810
- 457 Mantua, N. J., Hare, S. R., Zhang, Y., Wallace, J. M., & Francis, R. C. (1997,
 458 June). A Pacific Interdecadal Climate Oscillation with Impacts on Salmon
 459 Production. *Bull. Am. Meteorol. Soc.*, *78*(6), 1069–1080. Retrieved

- 460 from <http://journals.ametsoc.org/bams/article/78/6/1069/55942/>
461 A-Pacific-Interdecadal-Climate-Oscillation-with doi: 10.1175/
462 1520-0477(1997)078<1069:APICOW>2.0.CO;2
- 463 Mariotti, A., Baggett, C., Barnes, E. A., Becker, E., Butler, A., Collins, D. C.,
464 ... Albers, J. (2020, May). Windows of Opportunity for Skillful Forecasts
465 Subseasonal to Seasonal and Beyond. *Bull. Am. Meteorol. Soc.*, 101(5), E608–
466 E625. Retrieved from [http://journals.ametsoc.org/bams/article/101/](http://journals.ametsoc.org/bams/article/101/5/E608/345558/Windows-of-Opportunity-for-Skillful-Forecasts)
467 [5/E608/345558/Windows-of-Opportunity-for-Skillful-Forecasts](http://journals.ametsoc.org/bams/article/101/5/E608/345558/Windows-of-Opportunity-for-Skillful-Forecasts) doi:
468 10.1175/BAMS-D-18-0326.1
- 469 Mayer, K. J., & Barnes, E. A. (2021). Subseasonal Forecasts of Opportunity
470 Identified by an Explainable Neural Network. *Geophys. Res. Lett.*, 48(10),
471 e2020GL092092. Retrieved from [http://agupubs.onlinelibrary.wiley](http://agupubs.onlinelibrary.wiley.com/doi/abs/10.1029/2020GL092092)
472 [.com/doi/abs/10.1029/2020GL092092](http://agupubs.onlinelibrary.wiley.com/doi/abs/10.1029/2020GL092092) doi: 10.1029/2020GL092092
- 473 Meehl, G. A., Hu, A., Arblaster, J. M., Fasullo, J., & Trenberth, K. E. (2013,
474 September). Externally Forced and Internally Generated Decadal Climate
475 Variability Associated with the Interdecadal Pacific Oscillation. *J. Clim.*,
476 26(18), 7298–7310. Retrieved from [https://journals.ametsoc.org/](https://journals.ametsoc.org/view/journals/clim/26/18/jcli-d-12-00548.1.xml)
477 [view/journals/clim/26/18/jcli-d-12-00548.1.xml](https://journals.ametsoc.org/view/journals/clim/26/18/jcli-d-12-00548.1.xml) doi: 10.1175/
478 JCLI-D-12-00548.1
- 479 Meehl, G. A., Hu, A., & Teng, H. (2016, June). Initialized decadal prediction
480 for transition to positive phase of the Interdecadal Pacific Oscillation. *Nat.*
481 *Commun.*, 7(1), 11718. Retrieved from [http://www.nature.com/articles/](http://www.nature.com/articles/ncomms11718)
482 [ncomms11718](http://www.nature.com/articles/ncomms11718) doi: 10.1038/ncomms11718
- 483 Meehl, G. A., Richter, J. H., Teng, H., Capotondi, A., Cobb, K., Doblas-Reyes,
484 F., ... Xie, S.-P. (2021, April). Initialized Earth System prediction from
485 subseasonal to decadal timescales. *Nature Reviews Earth & Environment*,
486 2(5), 340–357. Retrieved from [https://www.nature.com/articles/](https://www.nature.com/articles/s43017-021-00155-x)
487 [s43017-021-00155-x](https://www.nature.com/articles/s43017-021-00155-x) doi: 10.1038/s43017-021-00155-x
- 488 Merryfield, W. J., Baehr, J., Batté, L., Becker, E. J., Butler, A. H., Coelho,
489 C. A. S., ... Yeager, S. (2020, June). Current and Emerging Developments in
490 Subseasonal to Decadal Prediction. *Bull. Am. Meteorol. Soc.*, 101(6), E869–
491 E896. Retrieved from [https://journals.ametsoc.org/view/journals/](https://journals.ametsoc.org/view/journals/bams/101/6/bamsD190037.xml)
492 [bams/101/6/bamsD190037.xml](https://journals.ametsoc.org/view/journals/bams/101/6/bamsD190037.xml) doi: 10.1175/BAMS-D-19-0037.1

- 493 Power, S., Casey, T., Folland, C., Colman, A., & Mehta, V. (1999, May). Inter-
494 decadal modulation of the impact of ENSO on Australia. *Clim. Dyn.*, *15*(5),
495 319–324. Retrieved from <https://doi.org/10.1007/s003820050284> doi: 10
496 .1007/s003820050284
- 497 Schulzweida, U. (2019, October). *Cdo user guide*. Retrieved from [https://doi.org/](https://doi.org/10.5281/zenodo.3539275)
498 [10.5281/zenodo.3539275](https://doi.org/10.5281/zenodo.3539275) doi: 10.5281/zenodo.3539275
- 499 Simpson, I. R., Deser, C., McKinnon, K. A., & Barnes, E. A. (2018, October). Mod-
500 eled and Observed Multidecadal Variability in the North Atlantic Jet Stream
501 and Its Connection to Sea Surface Temperatures. *J. Clim.*, *31*(20), 8313–8338.
502 Retrieved from [https://journals.ametsoc.org/view/journals/clim/31/](https://journals.ametsoc.org/view/journals/clim/31/20/jcli-d-18-0168.1.xml)
503 [20/jcli-d-18-0168.1.xml](https://journals.ametsoc.org/view/journals/clim/31/20/jcli-d-18-0168.1.xml) doi: 10.1175/JCLI-D-18-0168.1
- 504 Simpson, I. R., Yeager, S. G., McKinnon, K. A., & Deser, C. (2019, August).
505 Decadal predictability of late winter precipitation in western Europe through
506 an ocean–jet stream connection. *Nat. Geosci.*, *12*(8), 613–619. Retrieved
507 from <https://www.nature.com/articles/s41561-019-0391-x> doi:
508 [10.1038/s41561-019-0391-x](https://www.nature.com/articles/s41561-019-0391-x)
- 509 Toms, B. A., Barnes, E. A., & Ebert-Uphoff, I. (2020). Physically Interpretable
510 Neural Networks for the Geosciences: Applications to Earth System Variabil-
511 ity. *Journal of Advances in Modeling Earth Systems*, *12*(9), e2019MS002002.
512 Retrieved from [https://agupubs.onlinelibrary.wiley.com/doi/abs/](https://agupubs.onlinelibrary.wiley.com/doi/abs/10.1029/2019MS002002)
513 [10.1029/2019MS002002](https://agupubs.onlinelibrary.wiley.com/doi/abs/10.1029/2019MS002002) doi: 10.1029/2019MS002002
- 514 Toms, B. A., Barnes, E. A., & Hurrell, J. W. (2021, June). Assessing decadal pre-
515 dictability in an earth–system model using explainable neural networks. *Geo-*
516 *phys. Res. Lett.*, *48*(12). Retrieved from [https://onlinelibrary.wiley.com/](https://onlinelibrary.wiley.com/doi/10.1029/2021GL093842)
517 [doi/10.1029/2021GL093842](https://onlinelibrary.wiley.com/doi/10.1029/2021GL093842) doi: 10.1029/2021gl093842
- 518 Trenberth, K. E., & Fasullo, J. T. (2013, December). An apparent hia-
519 tus in global warming? *Earths Future*, *1*(1), 19–32. Retrieved from
520 <https://onlinelibrary.wiley.com/doi/10.1002/2013EF000165> doi:
521 [10.1002/2013ef000165](https://onlinelibrary.wiley.com/doi/10.1002/2013ef000165)
- 522 Trenberth, K. E., & Shea, D. J. (2006). Atlantic hurricanes and natural variability
523 in 2005. *Geophys. Res. Lett.*, *33*(12). Retrieved from [http://doi.wiley.com/](http://doi.wiley.com/10.1029/2006GL026894)
524 [10.1029/2006GL026894](http://doi.wiley.com/10.1029/2006GL026894) doi: 10.1029/2006gl026894
- 525 van der Velden, E. (2020, February). CMasher: Scientific colormaps for making ac-

- 526 cessible, informative and 'cmashing' plots. *The Journal of Open Source Soft-*
527 *ware*, 5(46), 2004. doi: 10.21105/joss.02004
- 528 Wu, S., Liu, Z., Zhang, R., & Delworth, T. L. (2011, February). On the observed
529 relationship between the Pacific Decadal Oscillation and the Atlantic Multi-
530 decadal Oscillation. *J. Oceanogr.*, 67(1), 27–35. Retrieved from [https://](https://doi.org/10.1007/s10872-011-0003-x)
531 doi.org/10.1007/s10872-011-0003-x doi: 10.1007/s10872-011-0003-x
- 532 Xie, S.-P., & Tanimoto, Y. (1998). A pan-Atlantic decadal climate oscilla-
533 tion. *Geophys. Res. Lett.*, 25(12), 2185–2188. Retrieved from [http://](http://agupubs.onlinelibrary.wiley.com/doi/abs/10.1029/98GL01525)
534 agupubs.onlinelibrary.wiley.com/doi/abs/10.1029/98GL01525 doi:
535 10.1029/98GL01525
- 536 Yeager, S. G., Danabasoglu, G., Rosenbloom, N. A., Strand, W., Bates, S. C.,
537 Meehl, G. A., ... Lovenduski, N. S. (2018, September). Predicting Near-Term
538 Changes in the Earth System: A Large Ensemble of Initialized Decadal Predic-
539 tion Simulations Using the Community Earth System Model. *Bull. Am. Meteo-*
540 *rol. Soc.*, 99(9), 1867–1886. Retrieved from [https://journals.ametsoc.org/](https://journals.ametsoc.org/bams/article/99/9/1867/70398/Predicting-Near-Term-Changes-in-the-Earth-System-A)
541 [bams/article/99/9/1867/70398/Predicting-Near-Term-Changes-in-the](https://journals.ametsoc.org/bams/article/99/9/1867/70398/Predicting-Near-Term-Changes-in-the-Earth-System-A)
542 [-Earth-System-A](https://journals.ametsoc.org/bams/article/99/9/1867/70398/Predicting-Near-Term-Changes-in-the-Earth-System-A) doi: 10.1175/BAMS-D-17-0098.1
- 543 Zhang, R., & Delworth, T. L. (2006). Impact of Atlantic multidecadal oscillations on
544 India/Sahel rainfall and Atlantic hurricanes. *Geophys. Res. Lett.*, 33(17). Re-
545 trieved from <http://doi.wiley.com/10.1029/2006GL026267> doi: 10.1029/
546 2006gl026267
- 547 Zhang, R., Sutton, R., Danabasoglu, G., Kwon, Y.-O., Marsh, R., Yeager, S. G.,
548 ... Little, C. M. (2019, June). A review of the role of the Atlantic merid-
549 ional overturning circulation in Atlantic multidecadal variability and asso-
550 ciated climate impacts. *Rev. Geophys.*, 57(2), 316–375. Retrieved from
551 <https://onlinelibrary.wiley.com/doi/10.1029/2019RG000644> doi:
552 10.1029/2019rg000644
- 553 Zhang, Y., Wallace, J. M., & Battisti, D. S. (1997, May). ENSO-like Inter-
554 decadal Variability: 1900–93. *J. Clim.*, 10(5), 1004–1020. Retrieved from
555 [https://journals.ametsoc.org/view/journals/clim/10/5/1520-0442](https://journals.ametsoc.org/view/journals/clim/10/5/1520-0442_1997_010_1004_eliv_2.0.co_2.xml)
556 [_1997_010_1004_eliv_2.0.co_2.xml](https://journals.ametsoc.org/view/journals/clim/10/5/1520-0442_1997_010_1004_eliv_2.0.co_2.xml) doi: 10.1175/1520-0442(1997)010<1004:
557 ELIV>2.0.CO;2